PAN POLSKA AKADEMIA NAUK

METROLOGY AND MEASUREMENT SYSTEMS

Index 330930, ISSN 0860-8229

www.metrology.pg.gda.pl

M&MS

ESTIMATION OF VEHICLE SIDESLIP ANGLE VIA PSEUDO-MULTISENSOR INFORMATION FUSION METHOD

Te Chen[1)], Long Chen[1,2)], Yingfeng Cai[1,2)], Xing Xu[1,2)]

1) *Jiangsu University, School of Automotive and Traffic Engineering, Zhenjiang 212013, China* (*ujschente@163.com*, *caicaixiao0304@126.com*, *xuxing@mail.ujs.edu.cn*)
2) *Jiangsu University, Automotive Engineering Research Institute, Zhenjiang 212013, China* (✉ *chenlong@ujs.edu.cn*, 0511 8879 7620)

Abstract

This paper presents a novel sideslip angle estimator based on the pseudo-multi-sensor fusion method. The kinematics-based and dynamics-based sideslip angle estimators are designed for sideslip angle estimation. Also, considering the influence of ill-conditioned matrix and model uncertainty, a novel sideslip angle estimator is proposed based on the wheel speed coupling relationship using a modified recursive least squares algorithm. In order to integrate the advantages of above three sideslip angle estimators, drawing lessons from the multisensory information fusion technology, a novel thinking of sideslip angle estimator design is presented through information fusion of pseudo-multi-sensors. Simulations and experiments were carried out, and effectiveness of the proposed estimation method was verified.

Keywords: vehicle state estimation, sideslip angle, recursive least squares, multi-sensor information fusion, pseudo-measurements.

1. Introduction

Advanced active safety control systems have been widely used for ground vehicles to prevent fatal accidents and guarantee safety [1–3]. An active safety system, of which the antilock brake system, the electronic stability program, the traction control system, as well as the adaptive cruise control and collision warning are examples, is significant to vehicle stability control during complicated conditions and severe manoeuvres. The sideslip angle of ground vehicles is defined as the angle between the vehicle longitudinal axis and the vehicle velocity vector. Lots of vehicle motion control systems need to monitor the sideslip angle dynamically, that is to say, the stable performance of vehicle motion control is dependent on precise and credible sideslip angle information [4–7]. Recently, the auxiliary driving and self-driving, with the advantage of vehicle autonomous security and reduced mobility cost, have attracted interest and become the object of considerable efforts from both researchers and companies [8–10], the estimation of sideslip angle being also important to the vehicle path-following and lateral stability control. However, since the sideslip angle estimation is hard and costly to achieve by sensors that a vehicle is equipped with, an appropriate design of sideslip angle estimator is essential.

Article history: received on Nov. 16, 2017; accepted on Mar. 29, 2018; available online on Sep. 30, 2018, DOI: 10.24425/123902.

During the past decade, lots of researchers have been engaged in the field of sideslip angle estimation, achieving some great results. The algorithms applied to sideslip angle observer design in prior studies can be classified as the Kalman-filter-based method [11–18], the nonlinear-observer-based method [19–24], the optimal estimation method [25–27], the information fusion estimation method [27–32], the robust estimation method [34–36] *et al*. The Kalman filter and the corresponding improved filter are widely used in the research on sideslip angle estimation. Doumiati established a nonlinear vehicle model and compared the performance of *extended Kalman filter* (EKF) and *unscented Kalman filter* (UKF) in sideslip angle estimation [11]. With the deepening of research and its complexity, based on the characteristics of the objects to be estimated, the researchers tend to design sideslip angle estimators as a combination of the Kalman filter and another advanced estimation theory. Boada proposed a novel sideslip angle estimation method with the integrated adaptive neuro-fuzzy inference system and an UKF algorithm [15]. Liu presented a vehicle state estimation strategy based on a combination of the minimum model error criterion and EKF to improve the estimation accuracy [18]. It can be found that most approaches aim to obtain an enhancement of the estimation performance, and some of them are also concerned with reduction of the estimation cost. In order to achieve a reliable and accurate estimation, some papers estimate the sideslip angle by a data fusion method using the redundancy of measurements, or through the means of a multi-mode iteration filter. Li studied a combined estimator including different forms of vehicle-model-based observers to estimate the sideslip angle, utilizing the redundant information of the global positioning system and an inertial measurement unit to ensure the estimation accuracy [32].

In this paper, a novel sideslip angle estimation method is presented. Based on the kinematic and dynamic equations, the kinematics-based and dynamics-based sideslip angle estimators were designed. Moreover, a novel form of sideslip angle estimator is proposed based on the wheel speed coupling relationship. Considering the influence of ill-conditioned matrix and model uncertainty, an improved *recursive least squares* (RLS) estimation algorithm is presented to achieve the unbiased estimation. Regarding the three forms of sideslip angle estimator design, drawing lessons from the multi-sensor fusion technology, a pseudo-multi-sensor fusion estimation method is proposed to estimate the sideslip angle, in which the estimations of three above-mentioned estimators are regarded as pseudo-measurements.

The rest of this paper is organized as follows. The three different forms of sideslip angle estimators are presented is Section 2. The sideslip angle estimation with the information fusion method is described in Section 3. The simulation results are provided in Section 4. The experimental verifications are presented in Section 5, followed by the conclusive remarks.

2. Different forms of sideslip angle estimator design

2.1. Kinematics-based estimator

The longitudinal acceleration and lateral acceleration are computed as:

$$\begin{cases} a_x = \dot{v}_x - v_y\gamma + w_1 \\ a_y = \dot{v}_y + v_x\gamma + w_2 \end{cases}, \tag{1}$$

where a_x is the longitudinal acceleration; a_y is the lateral acceleration; v_x is the longitudinal vehicle speed, v_y is the lateral vehicle speed; γ is the yaw rate; w_1 and w_2 are the corresponding

Gaussian white noise. Based on (1), the integral observer for longitudinal and lateral vehicle speed estimation is designed as:

$$\begin{cases} v_x = \int (a_x + v_y \gamma)\, dt \\ v_y = \int (a_y - v_x \gamma)\, dt \end{cases} . \tag{2}$$

Based on (2), the kinematics-based estimator is designed; utilizing the estimation, the sideslip angle is calculated as:

$$\beta = v_y / v_x . \tag{3}$$

2.2. Dynamics-based estimator

In this section, a schematic diagram of the 3 degree of freedom vehicle model in the longitudinal, lateral, and yaw directions is shown in Fig. 1. The origin of dynamic coordinate system $x0y$ fixed on the vehicle coincides with the vehicle gravity centre, the x axis is the longitudinal axis of the vehicle (the forward direction is positive), the y axis is the lateral axis of the vehicle (the right-to-left direction is positive). The pitch, roll, vertical motions and the suspension system of the vehicle are ignored. It is assumed that the mechanical properties of each tire are the same. The serial numbers 1, 2, 3, and 4 of the wheels are respectively corresponding to the front-left, the front-right, the rear-left and the rear-right wheel. The lateral velocity, yaw rate and sideslip dynamic equations of a four-wheel vehicle model can be expressed as:

$$\begin{cases} \dot{v}_x = r v_y + \dfrac{1}{m}\left[(F_{x1}+F_{x2})\cos\delta - (F_{y1}+F_{y2})\sin\delta + F_{x3} + F_{x4}\right] \\ \dot{v}_y = -\gamma v_x + \dfrac{1}{m}\left[(F_{x1}+F_{x2})\sin\delta + (F_{y1}+F_{y2})\cos\delta + F_{y3} + F_{y4}\right] \\ \dot{\gamma} = \dfrac{1}{I_z}\Big[(F_{x1}+F_{x2})l_f \sin\delta - (F_{y3}+F_{y4})l_r + (F_{y1}+F_{y2})l_f \cos\delta + (F_{y1}-F_{y2})b_f \sin\delta \\ \qquad -(F_{x1}-F_{x2})b_f \cos\delta - (F_{x3}-F_{x4})b_r\Big] \end{cases} , \tag{4}$$

where v_x is the longitudinal vehicle speed; v_y is the lateral vehicle speed; m represents the vehicle mass; δ is the steering angle of the front wheels; I_z stands for the moment of inertia. F_{xj} and F_{yj} $(j = 1,2,3,4)$ are the longitudinal and lateral forces of the jth tire, respectively. l_f and l_r are the distances from the vehicle gravity centre to the front and rear axle, respectively. b_f and b_r are the half treads of the front wheels and rear wheels, respectively.

A longitudinal force observer is proposed and applied to obtain the longitudinal force, and further details can be found in [4]. The semi-empirical magic formula of a tire model is used in order to estimate the lateral tire force. The lateral tire force can be calculated as:

$$F_y = D \sin\{C \arctan[B\alpha - E(B\alpha - \arctan(B\alpha))]\}, \tag{5}$$

where B is a stiffness factor; C is a curve shape factor; D is a peak factor; E is a curve curvature factor; α is the wheel side slip angle. The tire model parameters: B, C, D, E, are related to the

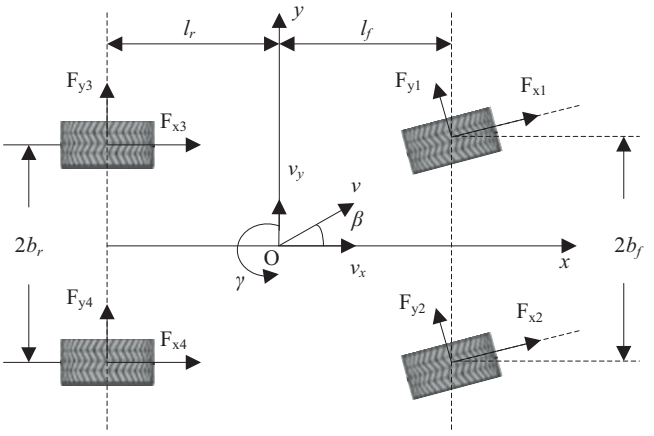

Fig. 1. A 3 degree of freedom vehicle model.

tire vertical load. The vertical load of each tire can be calculated as:

$$\begin{cases} F_{z1} = l_r\left(\dfrac{mg}{2l} + \dfrac{ma_y h}{2b_f l}\right) - \dfrac{ma_x h}{2l} \\ F_{z2} = l_r\left(\dfrac{mg}{2l} - \dfrac{ma_y h}{2b_f l}\right) - \dfrac{ma_x h}{2l} \\ F_{z3} = l_f\left(\dfrac{mg}{2} + \dfrac{ma_y h}{2b_r l}\right) + \dfrac{ma_x h}{2l} \\ F_{z4} = l_f\left(\dfrac{mg}{2} - \dfrac{ma_y h}{2b_r l}\right) + \dfrac{ma_x h}{2l} \end{cases}, \tag{6}$$

where F_{z1}, F_{z2}, F_{z3}, and F_{z4} are the vertical loads of corresponding tires; h is the height of the centre of gravity; g is the acceleration of gravity. The sideslip angle of each wheel can be obtained by:

$$\begin{cases} \alpha_1 = \delta - \arctan\dfrac{v_y + l_f\gamma}{v_x + b_f\gamma} \\ \alpha_2 = \delta - \arctan\dfrac{v_y + l_f\gamma}{v_x - b_f\gamma} \\ \alpha_3 = -\arctan\dfrac{v_y - l_r\gamma}{v_x + b_r\gamma} \\ \alpha_4 = -\arctan\dfrac{v_y - l_r\gamma}{v_x - b_r\gamma} \end{cases}. \tag{7}$$

The *extended Kalman filter* (EKF) is widely used to estimate the vehicle state. According to the 3 degree of freedom vehicle model and tire model, the generalized nonlinear state space equation can be expressed as:

$$\begin{cases} \dot{x}_v(t) = f(x_v(t), u_v(t)) + w(t) \\ y_v(t) = h(x_v(t), u_v(t)) + v(t) \end{cases}, \tag{8}$$

where $w(t)$ and $v(t)$ represent the process noise and measurement noise. The steps of EKF are given by:

1. The forecasting process.
   Calculate the forecast value:

$$\hat{x}_{k+1/k} = \hat{x}_{k/k} + f\left(\hat{x}_{k/k}\right)T + f(\hat{x}_{k/k})\,T^2/2. \tag{9}$$

   Calculate the variance of prediction error:

$$P_{k+1/k} = \varphi_k P_{k/k}\varphi_k^T + Q_k],, \tag{10}$$

   where $A(x_{k/k}) = \left.\dfrac{\partial f(x)}{\partial x}\right|_{x=\hat{x}_{k/k}}$, $\varphi_k = I + A\left(\hat{x}_{k/k}\right)T$.
2. The trimming process.
   Calculate the matrix of Kalman gain:

$$K_{k+1} = P_{k+1/k}H_{k+1}^T(H_{k+1}P_{k+1/k}H_k^T + R_{k+1})^{-1}. \tag{11}$$

   Update the state estimation

$$\hat{x}_{k+1/k+1} = \hat{x}_{k+1/k} + K_{k+1}\left[y_{k+1} - h(\hat{x}_{k+1/k})\right]. \tag{12}$$

   Update the error covariance

$$P_{k+1/k+1} = (I - K_{k+1}H_{k+1})P_{k+1/k}\,, \tag{13}$$

where $H = \partial h(x)/\partial x|_{x=\hat{x}(k/k)}$. Based on (4), the Kalman filter is devised for the estimation of longitudinal vehicle speed, lateral vehicle speed and yaw rate, where the input variable is $u_v = [\delta \;\; F_{x1} \;\; F_{x2} \;\; F_{x3} \;\; F_{x4} \;\; F_{y1} \;\; F_{y2} \;\; F_{y3} \;\; F_{y4}]^T$, the state variable is $x_v(t) = [v_x \;\; v_y \;\; \gamma]^T$, the measurement input is $y_v = [a_x \;\; a_y]^T$. Then, the vehicle sideslip angle can be obtained by (3), similarly.

2.3. Wheel speed coupling relationship-based estimator

The rotational speed of four wheels can be expressed as:

$$\begin{cases} n_1 = \left[(v_x + \gamma b_f)\cos\delta + (v_y + \gamma l_f)\sin\delta\right]/r \\ n_2 = \left[(v_x - \gamma b_f)\cos\delta + (v_y + \gamma l_f)\sin\delta\right]/r \\ n_3 = (v_x + \gamma b_r)/r \\ n_4 = (v_x - \gamma b_r)/r \end{cases}, \tag{14}$$

where n_1, n_2, n_3, and n_4 represent the speeds of corresponding wheels, respectively. r is the effective wheel radius. The observation equation of wheel speed coupling relationship system is written as:

$$Y = H\xi + V, \tag{15}$$

where Y is the observation vector; ξ is the state to be estimated; H is the measurement matrix, V is the zero mean white noise sequence. The corresponding vector and matrix are represented as:

$$Y = [n_1 \;\; n_2 \;\; n_3 \;\; n_4]^T, \qquad H = \begin{bmatrix} \frac{\cos\delta}{r} & \frac{\sin\delta}{r} & \frac{b_f\cos\delta + l_f\sin\delta}{r} \\ \frac{\cos\delta}{r} & \frac{\sin\delta}{r} & \frac{-b_f\cos\delta + l_f\sin\delta}{r} \\ \frac{1}{r} & 0 & \frac{b_r}{r} \\ \frac{1}{r} & 0 & -\frac{b_r}{r} \end{bmatrix}, \qquad \xi = [v_x \;\; v_y \;\; \gamma]^T.$$

The principle of RLS estimation is to provide the estimation of ξ ensuring the minimum observation error of quadratic function.

$$J = V^T V = \left[H\hat{\xi} - Y\right]^T \left[H\hat{\xi} - Y\right] = \min. \tag{16}$$

In accordance with, the estimation of ξ is expressed as:

$$\hat{\xi} = [H^T H]^{-1} H^T Y, \tag{17}$$

where a matrix $M = H^T H$ is called the information matrix.

In (14), theoretically, n_1, n_2, n_3, and n_4 show the ideal wheel speeds; it is impossible for an actual wheel speed to be precisely equal to the ideal wheel speed. Moreover, if matrix H is an ill-conditioned matrix, a little variation may cause a large deviation to the solution of RLS. Assuming there is a disturbance in (15), it can be expressed as:

$$Y + \Delta Y = (H + \Delta H) \cdot (\xi + \Delta\xi). \tag{18}$$

Unfolding and simplifying (18), we have:

$$\Delta Y = H \cdot \Delta\xi + \Delta H \cdot \xi + \Delta H \cdot \Delta\xi. \tag{19}$$

The sensitivity of RLS solution to an ill-conditioned matrix is represented by:

$$\Delta\xi = -H^{-1} \cdot \Delta H \cdot \xi - H^{-1} \cdot \Delta H \cdot \Delta\xi + H^{-1} \cdot \Delta Y. \tag{20}$$

Computing the norm of (20), according to the characteristics of the norm, we have:

$$\|\Delta\xi\| \le \|H^{-1}\| \cdot (\|\Delta H\| \cdot \|\xi\| + \|\Delta H\| \cdot \|\Delta\xi\| + \|\Delta Y\|). \tag{21}$$

It is reorganized as:

$$\left(1 - \|H^{-1}\| \cdot \|\Delta H\|\right) \frac{\|\Delta\xi\|}{\|\xi\|} \le \|H^{-1}\| \cdot \left(\frac{\|H\| \cdot \|\Delta Y\|}{\|H\| \cdot \|\xi\|} + \|\Delta H\|\right). \tag{22}$$

Defining $C = \|H^{-1}\| \cdot \|H\|$, we have:

$$\frac{\|\Delta\xi\|}{\|\xi\|} \le \frac{C}{1 - C\frac{\|\Delta H\|}{\|H\|}} \left(\frac{\|\Delta H\|}{\|H\|} + \frac{\|\Delta Y\|}{\|Y\|}\right). \tag{23}$$

It can be concluded that the greater C is, the more impressibleis.

According to the above-presented analysis, if we simultaneously enlarge the eigenvalue of ill-conditioned matrix H, the matrix C will have a certain extent of decrease, which contributes to the stability of RLS estimation.

Consequently, the ridge estimation method is used to suppress the influence of the ill-conditioned matrix in the estimation. The ridge estimation algorithm is essentially an improved RLS algorithm. Defining the eigenvalue increment of an ill-conditioned matrix H as K_1, and according to (17), the ridge estimation results can be expressed as:

$$\hat{\xi} = \left[H^T H + K_1 I\right]^{-1} H^T Y, \tag{24}$$

where I is the identity matrix. Thus, the ridge estimation method used for the vehicle state estimation can be written as:

$$\begin{cases} \hat{\xi}(k) = \hat{\xi}(k-1) + K_2\left(Y(k) - H(k)\xi(k-1)\right) \\ K_2(k) = \dfrac{P(k-1)H(k)}{\rho I + \left(H^T(k)H(k) + k_1 I\right)^T P(k-1)\left(H^T(k)H(k) + k_1 I\right)} \\ P(k) = \dfrac{1}{\rho}\left(I - K_2(k)H^T(k)\right)P(k-1) \end{cases}, \tag{25}$$

where $K_2(k)$ and $P(k)$ are the Kalman gain matrix and the covariance matrix, respectively, ρ is a forgetting factor used to balance the fast tracking ability and anti-jamming capability of the ridge estimation method. Then, according to (3), the sideslip angle estimation based on the wheel speed coupling relationship is obtained.

3. Sideslip angle estimation through information fusion

3.1. Novel thinking of pseudo-multi-sensor fusion method

Three forms of sideslip angle estimator are presented in Section 2. The kinematics-based estimator can obtain the sideslip angle estimation with less computational complexity, but the integral operation will result in the accumulation of noise and error. The dynamics-based estimator has a higher estimation accuracy and anti-interference performance. However, due to the prerequisite of nonlinear tire model, the amount of calculation is relatively larger and when the vehicle state changes rapidly, there will be some hysteresis in the estimation results. The wheel speed coupling relationship-based estimator is free from the influence of nonlinearity and saturation characteristics of the tire force, but its estimations are impressible with the variations and fluctuations of the wheel speed. Each one of the three estimators has its advantages and shortcomings, so they are applicable to different situations, thus an effective information fusion method will improve the accuracy and performance of estimation.

The multi-sensor fusion technology synthesizes the measured information from every sensor on the basis of some optimal fusion criteria to achieve the best fusion estimation. However, the vehicle sideslip angle is hard to measure, and it is costly and unpractical to equip a vehicle with multiple sensors for the estimation of only one vehicle state. Drawing lessons from the technical features of multi-sensor fusion technology, we propose a novel fusion estimation method and apply it to the sideslip angle estimation. In Section 2, three forms of sideslip angle estimators are presented based on different vehicle model and characteristic relationships. Here, every above estimator is regarded as a sensor and every estimated sideslip angle is regarded as a pseudo-measurement. The matrix weighted linear least variance optimal fusion algorithm is used to synthesize the estimated information and obtain the optimal sideslip angle estimation; we call this thinking of estimation as the pseudo-multi-sensor fusion method.

3.2. Observer design

A schematic diagram of the sideslip angle observer design is shown in Fig. 2. The yaw rate and sideslip angle estimation results of kinematics-based estimator, dynamics-based estimator and wheel speed coupling relationship-based estimator are marked as $x_1 = (\gamma_1, \beta_1)^T$, $x_2 = (\gamma_2, \beta_2)^T$, $x_3 = (\gamma_3, \beta_3)^T$, respectively. Actually, in x_1, the estimation of yaw rate is the real yaw rate; we regard it as the estimated value and use it to expand x_1. We regard the above-mentioned estimations as the measurements of sensors 1, 2, 3, and the real and optimally estimated vehicle states are denoted as x and x_0, respectively. Generally, we have:

$$E[x_i] = E[x] \quad (i = 0, 1, 2, 3). \tag{26}$$

The key problem of optimal estimation is achieving a weighted matrix W_i to satisfy the following condition:

$$x_0 = \sum_{i=1}^{3} W_i x_i \quad (i = 1, 2, 3). \tag{27}$$

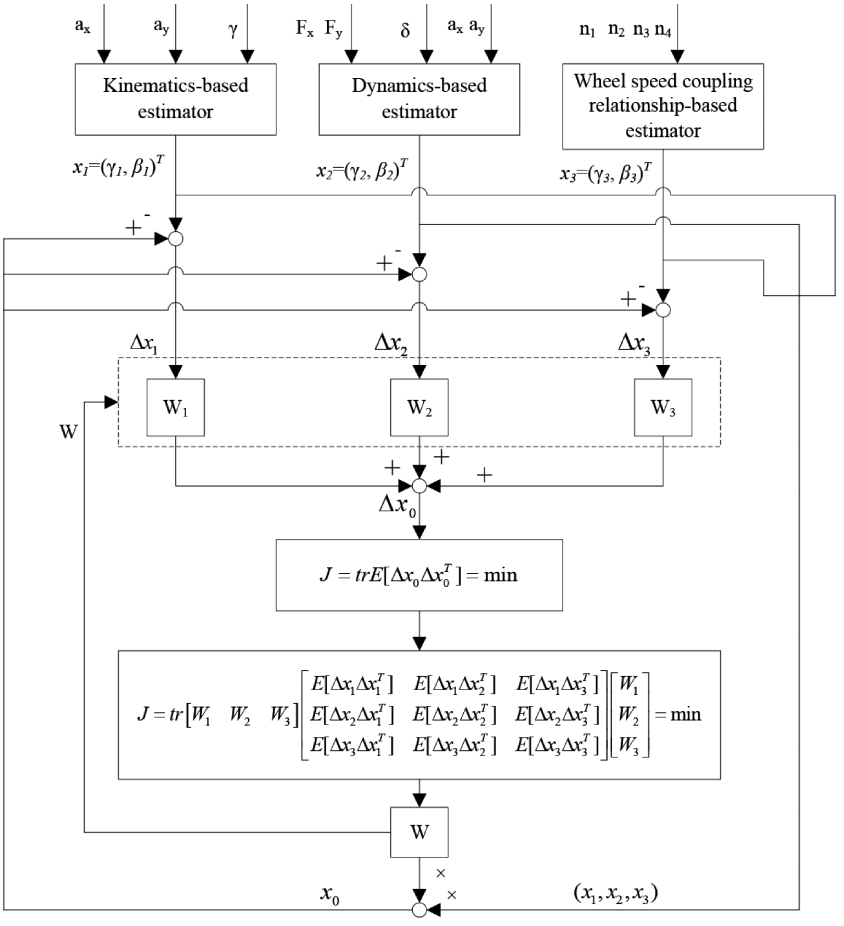

Fig. 2. A schematic diagram of the observer design.

Considering the unbiasedness of estimation, the constraint condition of (27) is $\sum_{i=1}^{3} W_i = I_{2\times 2}$, where $I_{2\times 2}$ denotes the identity matrix. The estimation errors between estimators 1, 2, 3 and the optimal fusion estimator can be written as $\Delta x_i = x_0 - x_i$; we have:

$$\Delta x_0 = \sum_{i=1}^{3} W_i \Delta x_i \qquad (i = 1, 2, 3). \tag{28}$$

Solving (27) aims to solving the problem:

$$J = E[\Delta x_0^T \Delta x_0] = trE[\Delta x_0 \Delta x_0^T] = \min. \tag{29}$$

Defining $W = [W_1 \;\; W_2 \;\; W_3]$ and $P = \begin{bmatrix} P_{11} & P_{12} & P_{13} \\ P_{21} & P_{22} & P_{23} \\ P_{31} & P_{32} & P_{33} \end{bmatrix}$, (29) is transformed to:

$$J = trWPW^T = \min, \tag{30}$$

where $P_{ii} = E[\Delta x_i \Delta x_i^T]$ is the variance matrix of the estimation error, $P_{ij} = E[\Delta x_i \Delta x_j^T]$ is the covariance matrix of the estimation error. The corresponding constraint condition of (30) is $W\lambda = I_{2\times 2}$ and $\lambda = [I_{2\times 2} \;\; I_{2\times 2} \;\; I_{2\times 2}]^T$. The problem is transformed into solving the minimization performance index of matrix W.

Using the Lagrange multiplier approach, an auxiliary function is created:

$$F = J + tr\sum_{i=1}^{2} \mu_i (W\lambda - I)\lambda_i, \tag{31}$$

where $\mu_i = [\mu_{i1} \;\; u_{i2}]$, $\lambda_i = [0 \;\; \cdots \;\; 0 \;\; 1 \;\; 0 \;\; \cdots \;\; 0]^T$, and in λ_i, the element of ith row is 1, the rest elements are 0. Defining $\partial F / \partial W = 0$, applying the matrix trace differential formula, we obtain:

$$2WP + \sum_{i=1}^{n} \mu_i^T (\lambda \lambda_i)^T = 0. \tag{32}$$

Defining $\Lambda = [\mu_1 \;\; \mu_2]^T = 2U^T$, we have:

$$\sum_{i=1}^{n} \mu_i^T (\lambda \lambda_i)^T = \Lambda^T \lambda^T. \tag{33}$$

Combining (32) and (33), we have:

$$PW^T + \lambda U^T = 0. \tag{34}$$

According to $\partial F / \partial \mu_i = 0$, it can be deduced as:

$$\lambda_i^T (W\lambda - I)^T = 0. \tag{35}$$

Merging (34) and (35), the matrix equation is given by:

$$\begin{bmatrix} P & \lambda \\ \lambda^T & 0 \end{bmatrix} \begin{bmatrix} W^T \\ U^T \end{bmatrix} = \begin{bmatrix} 0 \\ I_{2\times 2} \end{bmatrix}. \tag{36}$$

Calculating the inverse matrix of the partitioned matrix in (36), we obtain:

$$\begin{bmatrix} W^T \\ U^T \end{bmatrix} = \begin{bmatrix} P & \lambda \\ \lambda^T & 0 \end{bmatrix}^{-1} \begin{bmatrix} 0 \\ I_{2\times 2} \end{bmatrix} = \begin{bmatrix} P^{-1}\lambda(\lambda^T P^{-1}\lambda)^{-1} \\ -(\lambda^T P^{-1}\lambda)^{-1} \end{bmatrix}. \tag{37}$$

Thus, the weight matrix is obtained as:

$$W = \left(\lambda^T P^{-1}\lambda\right)^{-1} \lambda^T P^{-1}. \tag{38}$$

Finally, the optimal estimation results can be obtained as:

$$x_0 = W_1 x_1 + W_2 x_2 + W_3 x_3 \,. \tag{39}$$

4. Simulation results

To validate the effectiveness of the fusion estimation method proposed in this paper, simulations were carried out on a high-fidelity CarSim-Simulink joint simulation platform. CarSim was used to provide the whole vehicle model; the estimators were obtained in Matlab/Simulink. The vehicle parameters are listed in Table 1. For simplification, the kinematics-based estimator, dynamics-based estimator, wheel speed coupling relationship-based estimator and information fusion estimator are abbreviated as KBE, DBE, WBE and IFE, respectively.

Table 1. Parameters of vehicle.

Symbol	Parameters	Value and units
m	Vehicle mass	710 kg
r	Effective radius of wheel	0.245 m
l_f	Distances from vehicle gravity center to the front axle	0.795 m
l_r	Distances from vehicle gravity center to the rear axle	0.975 m
b_f, b_r	Half treads of the front(rear) wheels	0.775 m
C_f	Equivalent cornering stiffness of front wheel	60000 N/rad
C_r	Equivalent cornering stiffness of rear wheel	40000 N/rad

4.1. J-turn manoeuvre

In the simulation of J-turn manoeuvre, the road adhesion coefficient was set to 0.4, the vehicle speed was maintained at a constant of 10 m/s, and the steering wheel angle is shown in Fig. 3. Fig. 4 shows the estimation results of vehicle speed, vehicle lateral speed, yaw rate and sideslip angle, respectively. It can be found that WBE, DBE and KBE can estimate the vehicle speed precisely. But the lateral vehicle speed is better estimated by KBE and DBE than by WBE, the reason is that, since in the turning manoeuvre the rotational speeds of left and right wheels change rapidly, a slight disturbance will lead to an estimation error of the lateral vehicle speed. Moreover, the estimation results of KEB are obviously affected by noise. By contrast, the performance of DBE is relatively satisfactory in the tracking ability and noise immunity, but there is some delay in obtaining its estimation results. In the estimation of sideslip angle, the estimation result of IFE is more accurate than those obtained by other three estimators. As shown in Fig. 5, the weight coefficients of three estimators are time-varying, and when the sideslip angle

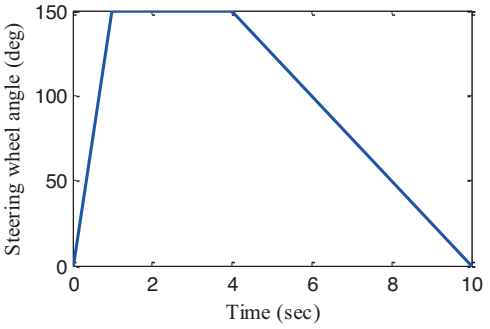

Fig. 3. The steering wheel angle.

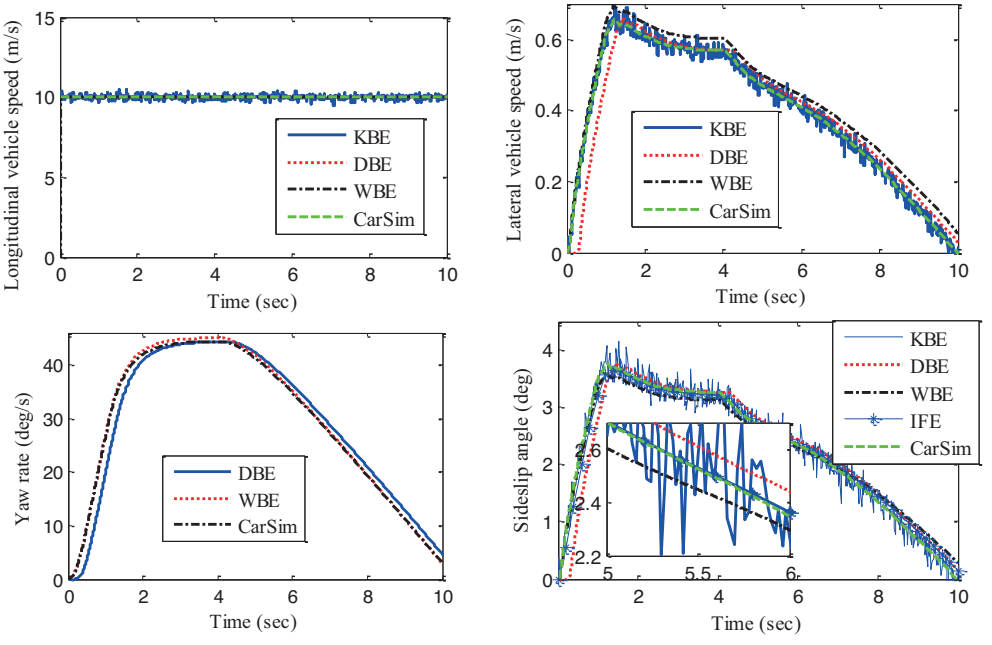

Fig. 4. Simulation results obtained in the J-turn manoeuvre.

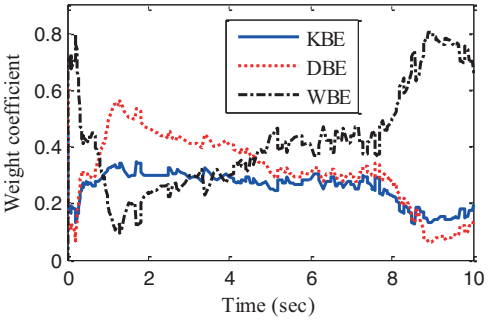

Fig. 5. Weight coefficients of three estimators in the J-turn manoeuvre.

is increasing, the weight coefficient of DBE is being reduced, whereas the weight coefficient of WBE is being increased accordingly. Due to the existence of noise, the expectation and variance of estimation error in KBE have a relatively severe fluctuation, so the weight coefficient of KBE is relatively low. It indicates that the proposed pseudo-multi-sensor fusion method improves the overall estimation performance.

4.2. Sine-turn manoeuvre

The sine-turn manoeuvre, as shown in Fig. 6, was carried out for further validation. In the simulation, the road adhesion coefficient was set to 0.8. The vehicle speed was maintained at a constant of 20 m/s. As shown in Fig. 7, same as in the case of the simulation results of J-turn

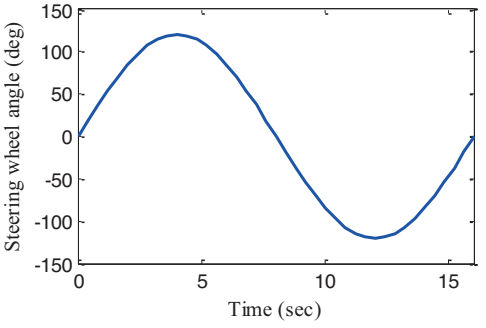

Fig. 6. The steering wheel angle.

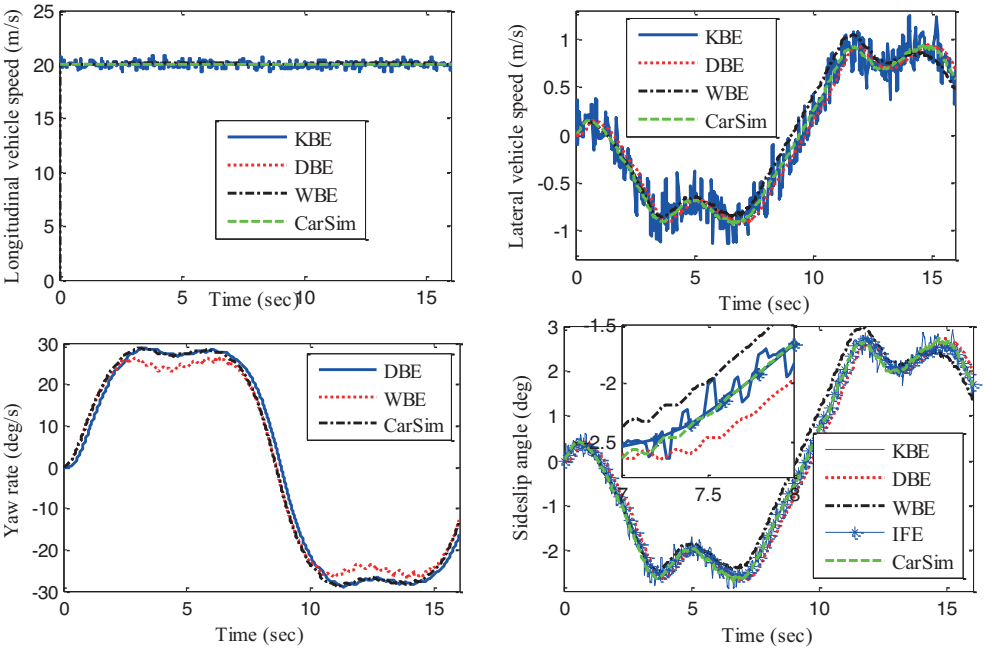

Fig. 7. Simulation results obtained in the sine-turn manoeuvre.

manoeuvre, the proposed IFE method exhibits a high estimation accuracy and a better estimation effect compared with the other three estimators. As shown in Fig. 8, the weight coefficients of three estimators are allocated in real time to obtain the optimal sideslip angle estimation, and the proposed fusion method performance achieved in simulation is satisfactory.

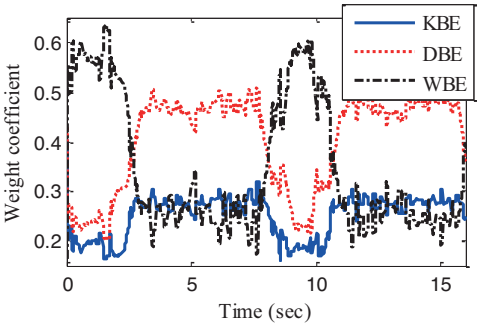

Fig. 8. Weight coefficients of three estimators in the sine-turn manoeuvre.

5. Experimental results

In this section, a road test is executed for further validation of the proposed estimation method in practice. Fig. 9 shows the scene of the road test, the experimental trajectory and the corresponding steering wheel angle, respectively. As shown in Fig. 10, in the estimation results of longitudinal vehicle speed and yaw rate, WBE, KBE and DBE can track the vehicle state with

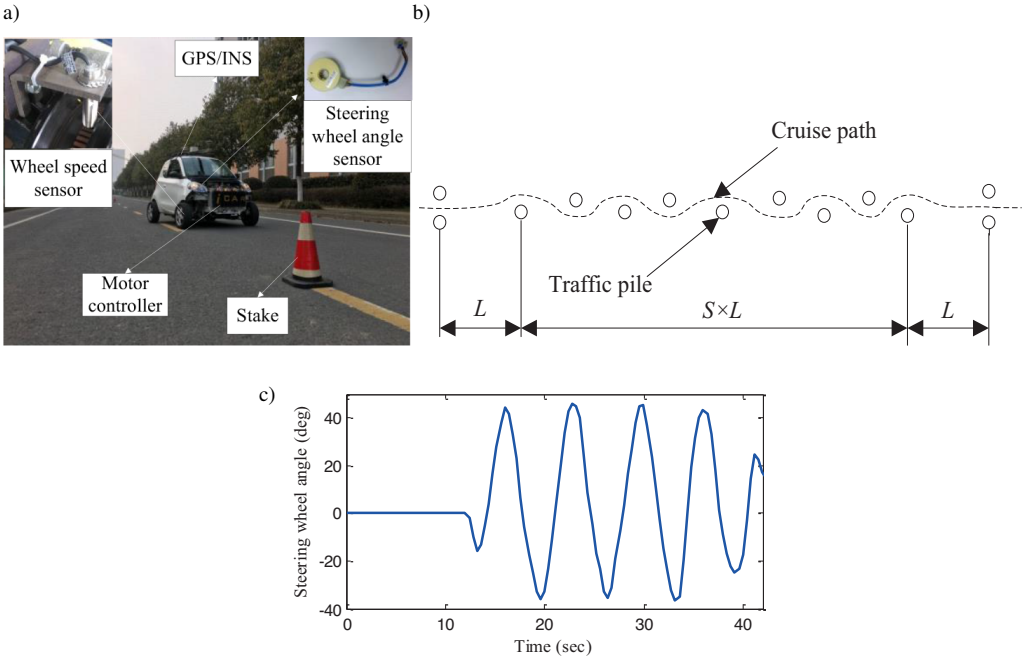

Fig. 9. The road test. The experimental vehicle (a); the experimental trajectory (b); the steering wheel angle (c).

a certain precision, and the advantages and defects of WBE, KBE and DBE are same as the ones obtained in the simulation. However, in the estimation results of lateral vehicle speed and sideslip angle, WBE is unstable and has a lot of violent swings, but considering the magnitudes of lateral vehicle speed and sideslip angle, the swings are acceptable. The estimation of KBE is relatively steady, but it is not immune to noise. By comparison, we can draw the conclusion that WBE is able to keep track of the variation trend but the estimation fluctuations are too large, KBE is relatively desirable if the influence of noise is not considered, DBE is stable when the vehicle manoeuvre and running condition is not very complicated, but the problem of time delay will affect the estimation effect. The design of IFE being a fusion and coordination of three estimators improves the estimation performance and is proved effective in practice.

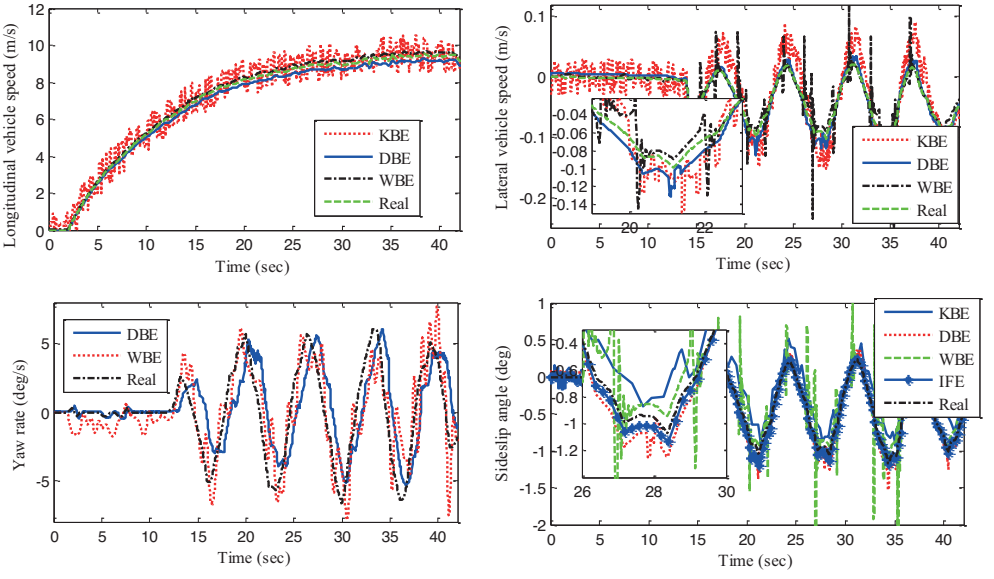

Fig. 10. Estimation results of the road test.

For further validation, the *root-mean-square* (RMS) error E_{RMS} between the measurement and estimation values is used for quantitative evaluation and can be computed with the following equation:

$$E_{RMS} = \sqrt{\frac{1}{N_s}\sum_{i=1}^{N_s}(\hat{x}_i - x_i)^2}, \tag{40}$$

where N_s is the number of samples; x_i and $\hat{x}_i$ denote the measured and estimated yaw rate and sideslip angle for the ith sample. Comparison of E_{RMS} for IFE and three different estimators regarding the estimation results of longitudinal vehicle speed, lateral vehicle speed, yaw rate and sideslip angle is shown in Table 2. It can be seen that E_{RMS} of IFE is smaller than that of KBE, DBE and WBE. Notice that the presented pseudo-multi-sensor fusion method guarantees the estimation accuracy and synchronously improves the stability of estimation system. In the road test, the vehicle speed and sideslip angle are relatively small, and the tires are still working in the linear area. Due to the limitations of experimental conditions and experimental sites, the severe experimental conditions for the tire nonlinear behaviour are unable to be obtained at present. It can be inferred that, if a tire works in the strong nonlinear region, the fusion estimation method

will reduce the weight coefficient of DBE to ensure the accuracy of estimation. Further tests and verifications will be carried out when the conditions are ripe enough.

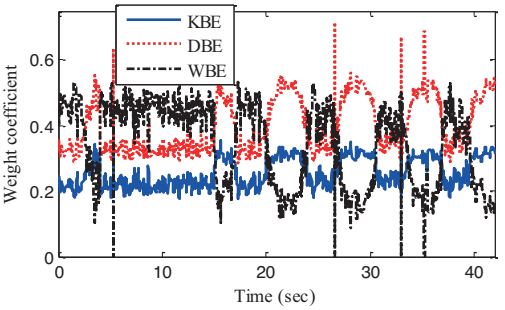

Fig. 11. Weight coefficients of three estimators in the experiment.

Table 2. Comparison of E_{RMS}.

E_{RMS}	Method			
	KBE	**DBE**	**WBE**	**IFE**
v_x	0.8764	0.2564	0.1697	×
v_y	0.2013	0.1322	0.1752	×
γ	×	0.5471	0.2071	×
β	0.6893	0.3346	0.3983	0.3217

6. Conclusion

This paper presents a novel sideslip angle estimator based on the proposed concept of pseudo-multi-sensor information fusion estimation method. The vehicle kinematic relationship and dynamic model are established, and the corresponding vehicle sideslip angle estimators are devised. In addition, a wheel speed coupling relationship-based sideslip angle estimator is designed on the basis of an improved RLS algorithm, in which the cases of ill-conditioned matrix and model uncertainty are considered. Then, drawing lessons from the multisensory information fusion technology, we regard the estimations obtained by the above three estimators as pseudo-measurements from sensors, and a pseudo-multi-sensor fusion estimation method is proposed to estimate the sideslip angle, in which the advantages of all three estimators can be colligated and applicable to different vehicle manoeuvres. Simulations of J-turn and DLC manoeuvres were carried out, their results show that the three above-mentioned sideslip angle estimators exhibit their own advantages and shortcomings, and the proposed pseudo-multi-sensor fusion estimation method can achieve more reliable and accurate estimation of the sideslip angle. For further validation, a road test was executed, and the proposed estimation method performance was verified. It needs to be further explained that, in the road test, the tires still work in the linear area due to the limitations of experimental conditions and experimental sites. In order to completely verify the fusion estimation method performance, further verifications will be carried out if the experiment conditions are ripe enough.

Acknowledgements

This work was supported by the National Natural Science Foundation of China (grant numbers U1664258 and U1564201), Six Major Talent Project of Jiangsu Province (grant number 2014-JXQC-004), 333 Project of Jiangsu Province (grant numberBRA2016445), Key R&D Plan of Jiangsu Province (grant number BE 2017129), and Natural Science Foundation of Jiangsu Province (grant number BK 20160525).

References

[1] Wang, R.R,, Hu, C., Wang, Z.J., Yan, F.J., Chen, N. (2015). Integrated optimal dynamics control of 4WD4WS electric ground vehicle with tire-road frictional coefficient estimation. *Mech. Syst. Signal Process*, 60–61, 727–741.

[2] Wang, R.R., Zhang, H., Wang, J.M. (2014). Linear parameter-varying controller design for four wheel independently-actuated electric ground vehicles with active steering systems. *IEEE Trans. Control. Syst. Technol*., 22(4), 1281–1296.

[3] Jo, C.H., Ko, J., Yeo, H., Kim, H. (2012). Cooperative regenerative braking control algorithm for an automatic-transmission-based hybrid electric vehicle during a downshift. *Proc IMechE Part D: J. Automobile Engineering*, (226), 457–467.

[4] Chen, T., Xu, X., Chen, L., Jiang, H.B., Cai, Y.F. (2018). Estimation of longitudinal force, lateral vehicle speed and yaw rate for four-wheel independent driven electric vehicles. *Mech. Syst. Signal Process*, 101, 377–388.

[5] Jin, X.J., Yin, G.D., Chen, N. (2015). Gain-scheduled robust control for lateral stability of four-wheel-independent-drive electric vehicles via linear parameter-varying technique. *Mechatronics*, 30, 286–296.

[6] Wang, R.R., Zhang, H., Wang, J.M., Yan, F.J., Chen, N. (2015). Robust lateral motion control of four-wheel independently actuated electric vehicles with tire force saturation consideration. *Journal of The Franklin Institute*, 352, 645–668.

[7] Nam, K., Fujimoto, H., Hori, Y. (2012). Lateral stability control of in-wheel-motor-driven electric vehicles based on sideslip angle estimation using lateral tire force sensors. *IEEE Trans. Veh. Technol*., 61(5), 1972–1985.

[8] Wang, R.R., Jing, H., Hu, C., Yan, F.J., Chen, N. (2016). Robust H∞ path following control for autonomous ground vehicles with delay and date dropout. *IEEE Trans. Intell. Transp. Syst*., 17(7), 2042–2049.

[9] Hu, C., Wang, R.R., Yan, F.J., Chen, N. (2016). Output constraint control on path following of four-wheel independently actuated autonomous ground vehicles. *IEEE Trans. Veh. Technol*., 65(6), 4033–4043.

[10] Wang, R.R., Hu, C., Yan, F.J., Chadli, M. (2016). Composite nonlinear feedback control for path following of four-wheel independently actuated autonomous ground vehicles. *IEEE Trans. Intell. Transp. Syst*., 17(7), 2063–2074.

[11] Doumiati, M., Victorino, A.C., Charara, A., Lechner, D. (2011). Onboard real-time estimation of vehicle lateral tire-road forces and sideslip angle. *IEEE/ASME Trans. Mechatronics*, 16(4), 601–614.

[12] Jin, X.J., Yin, G.D. (2015). Estimation of lateral tire-road forces and sideslip angle for electric vehicles using interacting multiple model filter approach. *Journal of The Franklin Institute*, 352, 686–707.

[13] Chen, B.C., Hsieh, F.C. (2008). Sideslip angle estimation using extended Kalman filter. *Vehicle Syst. Dyn*., 46(1), 353–364.

[14] Li, L., Song, J., Li, H.Z., Zhang, X.L. (2011). A variable structure adaptive extended Kalman filter for vehicle slip angle estimation. *Int. J. Veh. Des*., 56(1–4), 161–185.

[15] Boada, B.L., Boada, M.J.L., Diaz, V. (2016). Vehicle side slip angle measurement based on sensor data fusion using an integrated ANFIS and an Unscented Kalman Filter algorithm. *Mech. Syst. Signal Process*., 72, 832–845.

[16] Li, L., Jia, G., Ran, X., Song, J., Wu, K.H. (2014). Avariable structure extended Kalman filter for vehicle side slip angle estimation on a low friction road. *Veh. Syst. Dyn*., 52(2), 280–308.

[17] Liu, Y.H., Li, T., Yang, Y.Y., Ji, X.W., Wu, J. (2017). Estimation of tire-road friction coefficient based on combined APF-IEKF and iteration algorithm. *Mech. Syst. Signal Process*., 88, 25–35.

[18] Liu, W., He, H.W., Sun, F.C. (2016). Vehicle state estimation based on minimum model error criterion combining with extended Kalman filter. *Journal of The Franklin Institute*, 353, 834–856.

[19] Leung, K.T., Whildborne, J.F., Purdy, D., Dunoyer, A. (2011). A review of ground vehicle dynamic state estimations utilising GPS/INS. *Vehicle Syst. Dyn*., 49(1–2), 29–58.

[20] Baffet, G., Charara, A., Lechner, D. (2009). Estimation of vehicle sideslip, tire force and wheel cornering stiffness. *Control Eng. Pract*., 17(11), 1255–1264.

[21] Solmaz, S., Baslamish, S. (2012). A nonlinear sideslip observer design methodology for automotive vehicles based on a rational tire model. *Int. J. Adv. Manuf. Technol*., 60, 765–775.

[22] Ma, B., Liu, Y.H., Gao, Y.F., Yang, Y.Y., Ji, X.W., Bo, Y. (2016). Estimation of vehicle sideslip angle based on steering torque. *Int. J. Adv. Manuf. Technol*., DOI 10.1007/s00170-016-9426-2.

[23] Pi, D.W., Chen, N., Wang, J.X., Zhang, B.J. (2011). Design and evaluation of sideslip angle observer for vehicle stability control. *Int. J. Automotive Technology*, 12(3), 391–399.

[24] Li, B., Du, H., Li, W., Zhang, Y. (2015). Side-slip angle estimation based lateral dynamics control for omni-directional vehicles with optimal steering angle and traction/brake torque distribution. *Mechatronics*, 30, 348–362.

[25] Bevly, D.M., Ryu, J.H., Gerdes, J.C. (2006). Integrating INS sensors with GPS measurements for continuous estimation of vehicle sideslip, roll, and tire cornering stiffness. *IEEE Trans. Intell. Transport. Syst*., 7(4), 483–493.

[26] Li, X., Chan, C.Y., Wang, Y. (2016). A reliable fusion methodology for simultaneous estimation of vehicle sideslip and yaw angles. *IEEE Trans. Veh. Technol*., 65(6), 4440–4458.

[27] Madhusudhanan, A.K., Corno, M., Holweg, E. (2016). Vehicle sideslip estimator using load sensing bearings. *Control Eng. Pract*., 54, 46–57.

[28] Leung, K.T., Whildborne, J.F., Purdy, D., Barber P. (2011). Road vehicle state estimation using low-cost GPS/INS. *Mech. Syst. Signal Process*., 25(6), 1988–2004.

[29] Nam, K., Oh, S., Fujimoto, H. Hori, Y. (2013). Estimation of sideslip angle and roll angles of electric vehicles using lateral tire force sensors through RLS and Kalman filter approaches. *IEEE Trans. Ind. Electron*., 60(3), 988–1000.

[30] Yoon, J.H., Peng, H. A cost-effective sideslip estimation method using velocity measurements from two GPS receivers. *IEEE Trans. Veh. Technol*., 63(6), 2589–2599.

[31] Tuononen, A.J. (2009). Vehicle lateral state estimation based on measured tyre forces. *Sensors*, 9, 8761–8775.

[32] Li, X., Song, X, Chan CY. (2014). Reliable vehicle sideslip angle fusion estimation using low-cost sensors. *Measurement*, 51, 241–258.

[33] Yoon, J.H., Li, S.E., Ahn C. (2016). Estimation of vehicle sideslip angle and tire-road friction coefficient based on magnetometer with GPS. *Int. J. Automotive Technology*, 17(3), 427–435.

[34] Yoon, J.H., Peng, H. (2014). Robust vehicle sideslip angle estimation through a disturbance rejection filter that integrates a magnetometer with GPS. *IEEE Trans. Intell. Transp. Syst*., 15(1), 191–204.

[35] Zhang, B.J., Du, H.P., Lam, J., Zhang, N., Li, W.H. (2016). A novel observer design for simultaneous estimation of vehicle steering angle and sideslip angle. *IEEE Trans. Ind. Electron*., 63(7), 4357–4365.

[36] Zhang, H., Huang, X.Y., Wang, J.M., Karimi, H.R. (2015). Robust energy-to-peak sideslip angle estimation with applications to ground vehicles. *Mechatronics*, 30, 338–347.